Transmit-array antenna with aberration-free scanning

Artur A. Alves, Student Member, Carlos A. Fernandes, Senior Member, Sérgio A. Matos, Senior Member

***Abstract*—Beam steering is a vital feature of millimeter wave antennas in the context of satellite-on-the-move applications. The main challenge is to find cost-effective solutions compliant with the stringent antenna requirements of satellite communications. When compared with the electronic steering, mechanical scanning can greatly reduce the cost of the terminal. However, intrinsic aberrations of this approach need to be carefully managed. This thesis presents a new mechanical scanning design approach for transmit-array (TA) antennas. Usually, the TA phase correction is derived from a conversion of an incident spherical wave into a plane wave. In this work, an incoming Gaussian beam is considered instead. A Physical Optics (PO) analysis reveals that, in this ideal conditions, aberration-free scanning could be achieved. This concept is implemented by placing a thin dielectric lens in front of a horn antenna in order to produce the Gaussian illumination. Both the TA and shaping lens are manufacture using Fuse Deposition Modelling (FDM) 3D-printing in Polylactic Acid (PLA). The TA was design for a F/D of 0.71 using dielectric unit cells with a transmission loss lower than 1.84 dB, resulting in aperture of 195 mm $\times$ 145 mm and thickness from 0.4 mm to 14.2 mm. The fabricated antenna presented a maximum gain of 27.7 dBi at 30 GHz, with a scan loss of 3.8 dB for a 51.6 degrees elevation scanning. When comparing with a traditional scanning approach with the same F/D, the proposed approach allow a significant reduction of the overall side lobe levels (SLL) in the entire scanning range (SLL $<$ -16 dB).**

***Index Terms*—Ka-band, Transmit-array, beam steering, Gaussian beam.**

I. Introduction

Satellite communications at millimeter frequencies (30-300 GHz) provide a solution to the demand for global access to worldwide broadband internet access. For earth to satellite connection to happen there needs to be an antenna at the ground or user terminal, which can be stationary or mobile, and another at the satellite terminal. Communications between mobile user terminals, such as terrestrial vehicles, ships and aircraft, and fixed satellites, use frequencies of 30/20 GHz, more specifically 29.5-30 GHz for up-link and 19.7-20.2 GHz for down-link [1]. At these high frequencies, high gain antennas need to maintain the link between the satellite and the user terminal and in the case of a mobile user terminal, the use of beam scanning or steering is necessary to direct the electromagnetic energy to the intended target and suppress it in the unwanted directions in order to avoid interference. From the multiple solutions for beam scanning, mechanical scanning is the most affordable and simplest, which is relevant for mass production, specially if made with additive manufacturing, or 3D printing, with a low cost material.

For these requirements TA antennas are good solutions as they can be compact, lightweight and produce high gain. If produced by 3D printing they can also be very low cost and easily manufactured and beam steering can be achieved by displacement of the feed. However, as this displacement increases it results in beam aberrations which reduce the gain and thus limit the scanning performance. This dissertation proposes a new design of a TA antenna that addresses the aforementioned objectives and operates at Ka-band uplink [29.5, 30GHz]. The reduction of the beam aberrations is accomplished by making modifications to the usual concept of a TA antenna. The objectives of this work were to design the proposed antenna and show the that its concept works numerically and to develop a working prototype.

II. Formulation and Methods

Fig. 1 shows the working principle of a generic TA. The feed is located at the plane $z = 0$ and is being illuminated by a source at $(a, 0, -F)$, F being the focal distance and a being the feed translation, that is the distance from the origin $x = 0$. The output zenith angle, $\alpha(a)$ of the planar wavefront, depends on the feed translation a, which means that by translating the feed (or the lens), the output angle $\alpha(a)$ will change, thus achieving beam scanning.

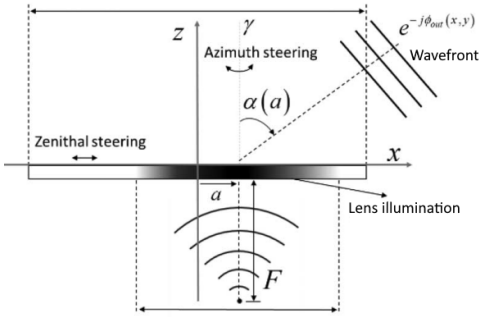

Fig. 1. Lens working principle, adapted from [2].

To get a collimated beam the TA needs to introduce a phase correction $\phi_{lens}(x, y, f)$, dependent on the the position on the TA and the frequency used,

$$\phi_{lens}(x, y, f) = k_0 r(x, y) \tag{1}$$

where $k_0 = 2\pi f/c$ is the free space wave number and r(x,y) is the element that counteracts the incident wave from the feed so as to obtain a collimated outgoing planar wave front and it adds an arbitrary tilt angle $\alpha(a)$, as seen in [2],

$$r(x, y) = -\phi_{in}(x, y)|_{a=0} + k_0 x \sin\alpha_0 \tag{2}$$

The phase of the outgoing wave is then given by the sum of the phase of the incoming wave and the phase delay imposed by the lens,

$$\phi_{out}(x,y) = \phi_{in}(x,y) - \phi_{in}(x,y)|_{a=0} + k_0 x \sin\alpha_0. \quad (3)$$

At $a = 0$, when the feed is in the central position, it reduces to

$$\phi_{out}(x,y)|_{a=0} = -k_0 x \sin\alpha_0, \quad (4)$$

which corresponds to a tilted main beam with zenith angle $\alpha(a=0) = \alpha_0$ as desired.

The dimensions of the lens are important to get the desired lens directivity. In [2] the lens directivity for a planar aperture, which represents the lens, with diameter D_A is approximated by

$$D_{max} = \eta\left(\frac{4\pi\sigma}{\lambda}\right)^2 tahn\left[\left(\frac{D_A}{4\sigma}\right)^2\right] cos\alpha_0 \quad (5)$$

and the minimum aperture diameter D_A by

$$D_A = \frac{1}{4\pi}\sqrt{\frac{8\tau\ln 10}{\tanh(\frac{\tau\ln\ln 10}{2})cos(\alpha_0)}\frac{D_{max}}{\eta}}, \quad (6)$$

where α_0 is replaced with the expression of α_a 20, η defines the aperture efficiency and τ corresponds to the edge field taper level $10^{-\tau}$.

This aperture diameter is also relevant for design parameter of the feed, such as the field taper to minimize spillover. Field taper is the difference in illumination between the highest point in the center and the lowest in the edge of the aperture and. Spillover is the radiation that misses the aperture and lowers the main beam gain. Because in this case the TA is used for beam scanning by translation of the feed, the length of the lens needs to be longer than the minimum aperture diameter so it can be properly illuminated by the feed.

An important parameter in the minimization of beam distortion is the focal distance F, represented in Fig. 1, which is the distance from the horn to the center of the lens. Increasing F can reduce beam distortion, SLL and scan loss due to nonlinear phase error reduction, approaching the $10log_{10}(cos\alpha_{max}/cos\alpha_0)$ limit obtained from (5), but as antenna compactness is an issue, F needs to be as low as possible. Scan loss is the difference in gain between the two positions with the highest and lowest gain.

To introduce the required phase delay along the lens the TA is composed of discrete phase shifting unit cells. These cells impose a spacial discretization, that is, the in plane dimensions of each cell, which are smaller than the wavelength, and a phase discretization, that is how many intervals in the $[0, 360°]$ are required. Unit cells are usually designed considering an infinite periodic structure of identical cells, in order to account for mutual coupling which happens in the actual lens. However, adjacent cells in the lens won't be equal and larger phase transitions between adjacent cells can lead to larger losses in the lens.

A. Spherical source transmit-array

A typical TA fed by an incident electric field illuminating the lens has spherical phase distribution

$$\phi_{in}(x,y) = k_0\sqrt{(x-a)^2 + y^2 + F^2}. \quad (7)$$

Using 3 to express the output phase for this $\phi_{in}(x,y)$,

$$\begin{aligned}\phi_{out}(x,y) = k_0\sqrt{(x-a)^2 + y^2 + F^2} - \\ - k_0\sqrt{x^2 + y^2 + F^2} + k_0 x \sin\alpha_0\end{aligned} \quad (8)$$

In [2] function (8) is analyzed for $y = 0$, $\alpha_0 = 0$ and a feed offset of $a = -0.3F$ to better understand the factors influencing the antenna beam scanning performance.

The phase distribution exhibits a linear behavior around the point $(x = \frac{a}{2}, y = 0)$. Therefore, a first-order Taylor expansion of (8) is performed in [2] around this point. It is expressed in (9) as a sum of a linear term ϕ_l, which just tilts the main beam, with ϕ_{nl} representing all the remaining nonlinear terms responsible for phase aberrations.

$$\begin{aligned}\phi_l(x) &= \frac{k_0 F(a/F)^2}{\sqrt{(}4 + (a/F)^2)} + k_0\Big(\sin\alpha_0 - \frac{2a/F}{\sqrt{(}4 + (a/F)^2)}\Big)x \\ \phi_{nl}(x,y) &= \phi_{out}(x,y) + \phi_l(x)\end{aligned} \quad (9)$$

The output beam zenith angle $\alpha(a)$ is estimated from ϕ_l as

$$\alpha(a) = \arcsin\left[\sin\alpha_0 - \frac{2a/F}{\sqrt{(}4 + (a/F)^2)}\right], \quad (10)$$

which confirms that $\alpha(0) = \alpha_0$. The predicted zenith angle, or tilt, depends only on the ratio between the feed offset a and the focal distance F, which means that different values of F but the same values of a/F the resulting tilt will be the same.

A preliminary PO analysis was done for a few a/F values to better understand these effects. The PO used was KH3D near [3], which is able to calculate the radiation pattern of an arbitrarily shaped aperture, defined by a set of node points over a grid. KH3D near evaluates the aperture near- or far-field radiation in magnitude and phase at any arbitrary distance from the specified aperture, in rectangular or spherical coordinates.

Fig. 2 shows an example of the the theoretical zenith beam direction given by (10) (dashed blue curve) and the curves obtained through PO analysis which include the nonlinear phase error (solid orange curves) versus the normalized feed offset, a/F, for two different values for α_0. When $\alpha_0 \neq 0$ less displacement of the feed, a, is necessary to obtain a higher beam tilt and thus there are lower aberrations then with $\alpha_0 = 0$ as these are larger for larger displacements of the feed.

In the example of Fig. 2, for $\alpha_0 = 30°$, the zenith scanning range $\alpha = [0, 50°]$ corresponds, according to (10), to the feed offset $a \in [-0.25F, 0.56F]$ (see dashed blue curve in Fig. 2.

The radiation pattern for a fixed focal distance F and varying feed translation a is represented in Fig. 3. The dashed black curve represents the maximum value of the radiation pattern if nonlinear phase error was zero (5).

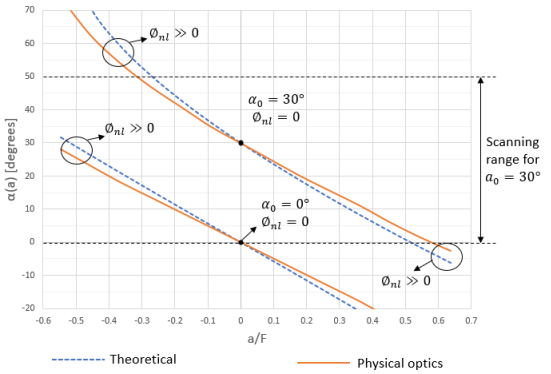

Fig. 2. Zenith beam direction as function of the feed offset (theoretical 10 and PO results) for a spherical wave source.

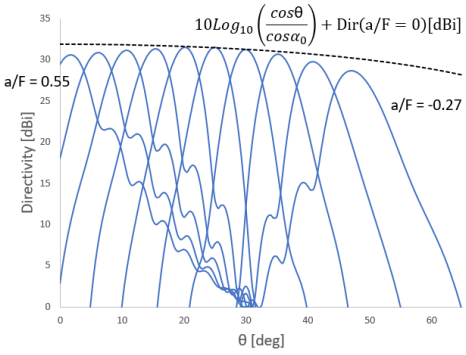

Fig. 3. Directivity obtained by PO radiation pattern for the feed offset in the interval $a/F \in [-0.27, 0.55]$ with 0.09 steps. The dashed black curve represents the maximum normalized directivity as function of θ considering $\phi_{nl} = 0$.

The effect of the ϕ_{nl} term is noticeable for large $a/F > 0$ values. As the feed moves from the central position the effect of the nonlinear term becomes more significant as can be seen from the decay in directivity from the value which considers nonlinear phase error to be zero (dashed black curve) and from the aberrations in the main beams. This directivity decay for lower zenith angles ($a/F > 0$) is explained by the phase error and increasing spillover, effects that counteract the increase of the effective aperture size. The directivity decay with the increase of the zenith angle, for $a/F < 0$ can be partly explained by the $cos(\alpha)$ reduction of the effective aperture size caused by the beam tilt. This directivity, obtained with PO, is higher than the target specification because it does not take into account effects like unit cells reflections and insertion losses, or phase errors originated by the primary feed.

To eliminate the mentioned effects of non linear phase errors, the decay in directivity and the aberrations, a different feed is proposed: a Gaussian beam. The design of a Gaussian beam source TA is studied in the next subsection.

B. Gaussian beam source transmit-array

Gaussian beams are beams of electromagnetic radiation where the electric field profile in a plane perpendicular to the beam axis can be described with a Gaussian function. The mathematical expression for the electric field amplitude of a Gaussian beam is a solution to the paraxial Helmholtz equation. Assuming polarization in the x direction and propagation in the $+z$ direction the electric field in phasor notation is given by

$$\mathbf{E}(r,z) = E_0 \frac{w_0}{w(z)} e^{\frac{-\sqrt{(x^2+y^2)}}{w(z)^2}} e^{-i(kz+k\frac{r^2}{2R(z)}-\psi(z))} \tag{11}$$

where $R(z)$ can be expressed as,

$$R(z) = z\left[1 + (\frac{z_r}{z})^2\right] \tag{12}$$

and z_r as

$$z_r = \frac{\pi w_0^2}{\lambda}. \tag{13}$$

For the case of the Gaussian beam, the expression of the wave phase at the lens input, at a distance of F is given by

$$\phi_{in}(x,y) = k_0\left[F + \frac{(x-a)^2+y^2}{2F\left[1+(\pi w_0^2/(\lambda F))^2\right]}\right] \tag{14}$$

where a is the feed offset along the x coordinate and F is the focal distance.

The phase needed to be introduced by the lens is given by

$$\begin{aligned}\phi_{lens}(x,y) =& \phi_{out} - \phi_{in} = \\ & - k_0\left[F + \frac{x^2+y^2}{2F\left[1+(\pi w_0^2/(\lambda F))^2\right]}\right] + k_0 x \sin\alpha_0.\end{aligned} \tag{15}$$

The phase of the outgoing wave is simply given by the sum of $\phi_{in}(x,y)$ and $\phi_{lens}(x,y)$,

$$\begin{aligned}\phi_{out}(x,y) =& k_0\left[F + \frac{(x-a)^2+y^2}{2F\left[1+(\pi w_0^2/(\lambda F))^2\right]}\right] \\ & - k_0\left[F + \frac{x^2+y^2}{2F\left[1+(\pi w_0^2/(\lambda F))^2\right]}\right] + k_0 x \sin\alpha_0.\end{aligned} \tag{16}$$

At $a = 0$ it also reduces to

$$\phi_{out}(x,y)|_{a=0} = k_0 x \sin\alpha_0. \tag{17}$$

Again, the function for the phase output, 16, is analyzed for $y = 0$, $\alpha_0 = 0$ and a feed offset of $a = -0.3F$.

$$\begin{aligned}\phi_{out}(x) =& -k_0[F + \frac{(x+0.3F)^2}{2R(F)}] + k_0\left[F + \frac{x^2}{2R(F)}\right] \\ =& \frac{-k_0}{2}\frac{0.6x + 0.09F}{1+(\frac{z_r}{F})^2}\end{aligned} \tag{18}$$

The function 26 and is linear so, for a Gaussian beam feed, the output beam will not suffer distortion due to nonlinear phase error effects. But as for the spherical source wave, a first-order Taylor expansion of 16 is performed around this point. It is expressed as a sum of a linear term ϕ_l , which just

tilts the main beam, with ϕ_{nl} representing all the remaining nonlinear terms responsible for phase aberrations

$$\begin{cases} \phi_l(x) = \dfrac{k_0 F (a/F)^2}{2\left[1+(\pi w_0^2/(\lambda F))^2\right]} - \\ \qquad - k_0\left(\dfrac{a/F}{\left[1+(\pi w_0^2/(\lambda F))^2\right]} - \sin\alpha_0\right)x \\ \phi_{nl}(x,y) = \phi_{out}(x,y) + \phi_l(x) \end{cases} \tag{19}$$

The output beam angle $\alpha(a)$ can be estimated from 16 as

$$\alpha(a) = \arcsin\left[\sin\alpha_0 - \frac{a/F}{\left[1+(\pi w_0^2/(\lambda F))^2\right]}\right] \tag{20}$$

and, as with a spherical feed, $\alpha(0) = \alpha_0$. Unlike in the case of a spherical wave source, the zenith angle doesn't depend only on the ratio between the feed offset a and the focal distance F, a/F, as it also depends on F alone, on the wavelength and thus the frequency, and on the beam waist, w_0, of the Gaussian beam. However, varying the value of F while keeping the same a/F will have little impact on the tilt, according to (20), but the greater the value of F, the greater the feed displacement a will have to be to keep the same a/F and approximately the same tilt.

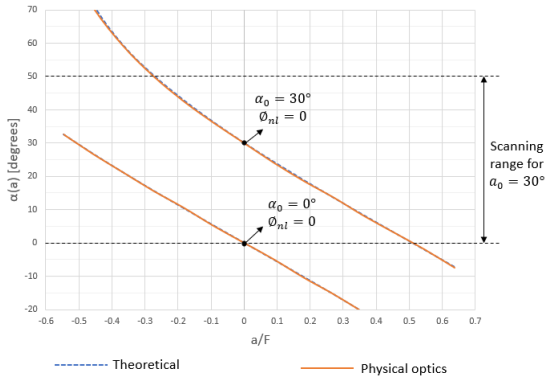

Fig. 4. Zenith beam direction as function of the feed offset (theoretical 10 and PO results) for a Gaussian beam source.

As for the spherical source TA, a preliminary PO analysis was done for a few a/F values to better understand these effects. Fig. 4 shows an example of the the theoretical zenith beam direction given by (20) (dashed blue curve) and the curves obtained through PO analysis which include the non-linear phase error (solid orange curve) versus the normalized feed offset, a/F, for two different values for α_0. Unlike in the case of the spherical wave source, there is no noticeable effect of the ϕ_{nl} term.

In the example of Fig. 4, for $\alpha_0 = 30°$, the zenith scanning range $\alpha = [0, 50°]$ corresponds, according to 10, to the feed offset $a \in [-0.27F, 0.51F]$, for $F = 110$ mm, (dashed blue curve).

The radiation pattern for a fixed focal distance $F = 110$ mm and varying feed translation a is represented in Fig. 5. The dashed black curve represents the maximum value of the radiation pattern if nonlinear phase error was zero (5).

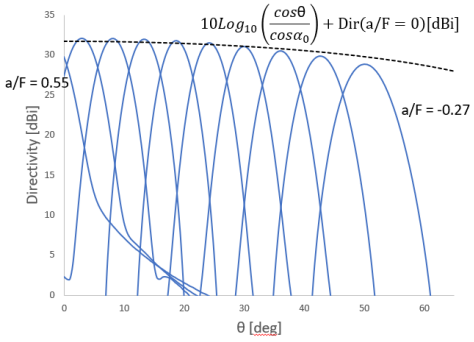

Fig. 5. Directivity obtained by PO radiation pattern for the feed offset in the interval $a/F \in [-0.27, 0.55]$ with 0.09 step size. The dashed black curve represents the maximum normalized directivity as function of θ considering $\phi_{nl} = 0$.

In the case of the Gaussian beam source in Fig. 5 there is no directivity decay for lower zenith angles ($a/F > 0$), as there is no noticeable nonlinear phase error, as indicated in (4), and no aberrations in the main beams. This is why a Gaussian beam source is being proposed for a beam scanning TA.

To produce a Gaussian beam the Gaussian beam's waist position and size, z and w_0, have to be defined. These can be chosen considering the desired edge field taper which can be defined by the ratio of the incident field intensity at the "edge" of the lens aperture and in its center.

$$T(dB) = 20log_{10}[\frac{|E(r,z)|}{|E(0,z)|}] = 20log_{10}e^{[-\frac{r}{w(z)}]^2} \tag{21}$$

Solving it to $w(z)$,

$$w(z) = \frac{r}{T(dB)^{0.5} ln(10^{0.5})^{0.5}} = \frac{r}{T(dB)^{0.5} 0.3393} \tag{22}$$

From $w(z)$, the beam waist at the central position, w_0, can be calculated from

$$w(z) = w_0\sqrt{1+\frac{z}{z_r}} \Leftrightarrow w_0^4 - w(z)^2 w_0^2 + \frac{F^2\lambda^2}{\pi^2} = 0 \tag{23}$$

Because the mathematical expression for the electric field amplitude of a Gaussian beam is a solution to the paraxial Helmholtz equation and the simulation tool used for simulations, Computer Simulation Technology - Microwave Studio (CST-MWS), uses a paraxial approximation that assumes

$$\begin{aligned} z_r &> 4\lambda/\pi \\ w_0 &> 2\lambda/\pi, \end{aligned} \tag{24}$$

these conditions are applied to the choice of the value of the beam waist w_0.

CST-MWS is a 3D electromagnetic analysis software package for designing, analyzing and optimizing electromagnetic components and systems.

III. Gaussian beam feed

To produce a Gaussian beam feed a thin dielectric lens was designed. This lens can be 3D printed and so the feed is simple and cheap to produce. It introduces a phase delay such as to produce a Gaussian beam shaped wave. This lens will be called Gaussian lens (GL) for simplicity. The geometry of the feed and its placement in relation to the main lens is represented in Fig. 6.

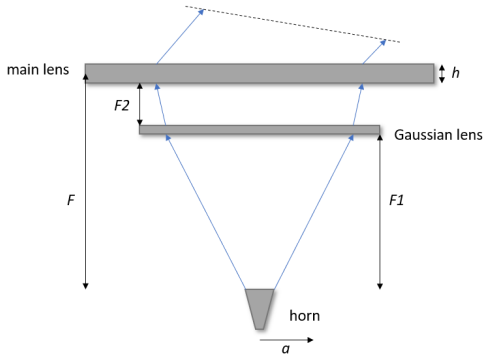

Fig. 6. Proposed solution working principle.

The input phase is that of a spherical wave for a distance $z = F_1$,

$$\phi_{in}(x,y) = k_0\sqrt{x^2+y^2+F_1^2} \tag{25}$$

The phase does not depend on the feed displacement a because the horn and the GL move together.

The output phase is that of a Gaussian beam

$$\phi_{out}(x,y) = k_0\left[F_1 + \frac{x^2+y^2}{2F_1\left[1+(\pi w_0^2/(\lambda F_1))^2\right]}\right]. \tag{26}$$

The phase delay introduced by the lens is the difference between the phases,

$$\begin{aligned}\phi_{lens}(x,y) =& k_0\left[F_1 + \frac{x^2+y^2}{2F_1\left[1+(\pi w_0^2/(\lambda F_1))^2\right]}\right]- \\ &- k_0\sqrt{x^2+y^2+F_1^2}.\end{aligned} \tag{27}$$

To design the GL the parameters of the Gaussian beam have to be defined, based on some conditions, which are a frequency of a 30 GHz, a taper of 15 dB on the surface of the main lens at $r = D_A/2 = 72.5$ mm and a focal distance $F = 110$ mm for the main lens. These conditions are used in Equations 22 and 23 and the parameters of the Gaussian beam are thus,

- $\lambda = c/f = 10$ mm
- $w_0 \approx 6.4$ mm from (23)
- $z_r \approx 12.9$ mm from (13)

Since the paraxial approximation imposes the minimum values of,

$$\begin{aligned}z_r > 4\lambda/\pi \Leftrightarrow z_r > 12.7mm \\ w_0 > 2\lambda/\pi \Leftrightarrow w_0 > 6.4mm,\end{aligned} \tag{28}$$

$w_0 = 6.5$ mm with a $z_r = 13.3$ mm can be used to satisfy both conditions and be close to a taper of 15 dB.

The focal distance for the GL, F_1, was defined by having a fixed value for the main lens focal distance, $F = 110$ mm, and studying the effect on the distance between the two lenses, F_2, with some PO simulations.

The focal distance for the GL, $F_1 = 30mm$. This value was chosen so as to leave enough distance between the two lenses, F_2, to avoid having too much reflections and also enough distance from the horn to the GL, F_1 to avoid beam distortion, while keeping a fixed value for the main lens focal distance, $F = 110mm$ and the targeted directivity of 29 dBi for the central position of the feed.

The height of the dielectric GL to introduce the necessary phase shift is given by (29).

$$\begin{aligned}\phi_{lens}(x,y) = \phi_{PLA}(x,y) + \phi_{air}(x,y) \Leftrightarrow \\ \Leftrightarrow h(x,y) = \frac{\phi_{lens}(x,y)/k_0 + h_{max}}{\sqrt{\epsilon_r}-1}\end{aligned} \tag{29}$$

where k_0 is the wave number and ϵ_r is the material's relative permittivity and $h_{max} = 20$ mm and $\phi_{lens}(x,y)$ is obtained from 27. A constant value was added to $\phi_{lens}(x,y)$ and $h(x,y)$ in order to obtain positive values for $h(x,y)$ as is represented. The minimum height was set to be at least 0.27 mm to be viable for 3D printing.

The 3D model of the lens, shown in 7, is made by making a 3D plot of the height with a radius of 67.5 mm. This radius should be smaller than the smallest section of the main lens, $D_A/2 = 72.5$ mm and small enough so that the height does not get too high on the border where the difference in phase gets larger (see Fig. 16) but large enough so that the incident phase in the TA lens is going through the GL and not around it. This puts a limitation on the feed displacement a, as it only enables to go so far as $a = -30$ mm and $a = 30$ mm because a higher offset would make it so part of the GL is not directly below the TA lens, which leads to high spillover.

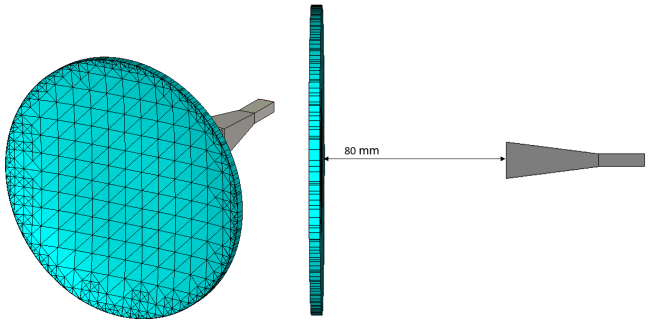

Fig. 7. Model of the Gaussian beam feed.

The feed composed by the GL and a horn with a gain of 14.7 dBi at 30 GHz was simulated in CST-MWS. The resulting E-field and farfield are represented (solid blue curves) in Figures 8 and 9 respectively. Superimposed to these are the same components but for an ideal Gaussian beam produced by a CST-MWS macro (solid orange curves). The designed feed E-field of the GL and horn shows good agreement with this

ideal feed, up until the borders of the GL at $x = \pm 67.5mm$, where a larger deviation becomes visible. The radiation pattern for the farfield directivity also shows good agreement for the two feeds, with a directivity of 14.9 dBi for the GL feed and of 15.5 dBi for the CST-MWS macro at $\theta = 0°$.

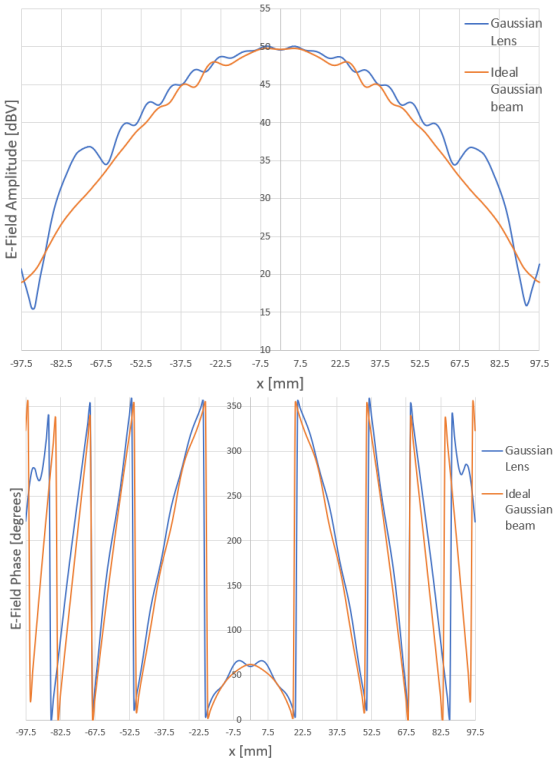

Fig. 8. E-field from GL and horn and from an ideal Gaussian beam produced by a CST-MWS macro.

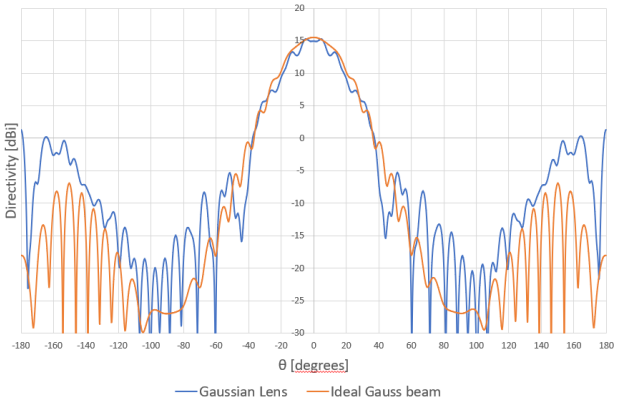

Fig. 9. Simulated farfield directivity radiation pattern for the feed offset in the interval $a/F \in [-0.27, 0.55]$ with 0.09 step size. The dashed black curve represents the maximum normalized directivity as function of θ considering $\phi_{nl} = 0$.

IV. Unit Cell Design

The role of the TA Lens is to introduce a phase shift such as to compensate the incident phase and also to introduce a beam tilt. The phase shift is obtained by the use of different unit cells. Two types of cells are used: parallelepipeds with a square base and a varying sized square shaped hole at the center through and through, with equivalent height and base (type 1), as seen in Fig. 10, and parallelepipeds with a square base with equivalent dimensions and varying height (type 2), as seen in Fig. 11.

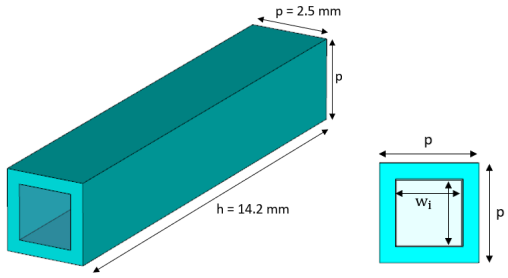

Fig. 10. Model of type 1 cell.

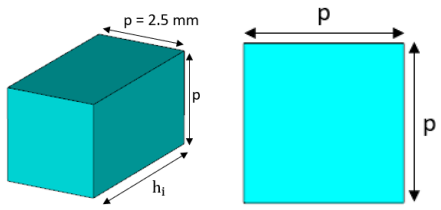

Fig. 11. Model of type 2 cell.

The unit cells are made of a thermoplastic material with dielectric properties, PLA, with a dielectric constant of $\epsilon_r = 2.9$ and a loss tangent of $tan\sigma = 0.018$ at 30 GHz.

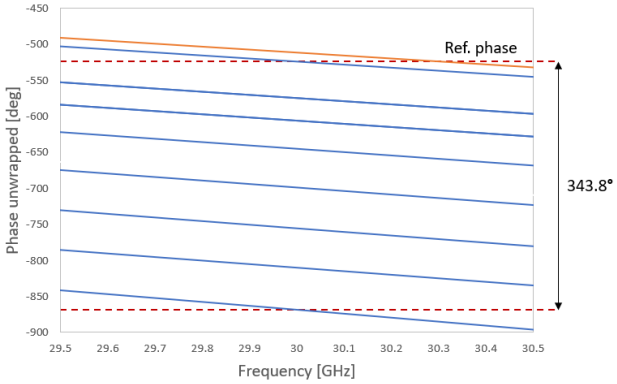

Fig. 12. Transmission coefficient S_{21} unwrapped phase for a sample of unit cells.

To obtain the phase introduced for each valued of w and h the model of each cell was built, separately, in CST-MWS. The boundaries of the cell were set to "Unit Cell", to simulate an infinite array of identical cells. Of course, this method has limitations as it doesn't represent exactly what happens in the actual lens, as the adjacent cells differ from each other, the incidence angle is different depending on the distance to the

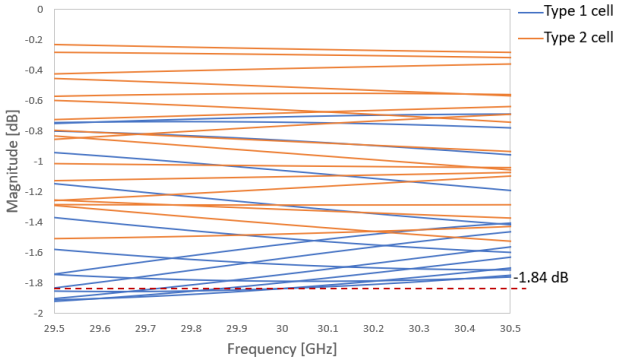

Fig. 13. Amplitude of the transmission coefficient $|S_{21}|$ for all unit cells.

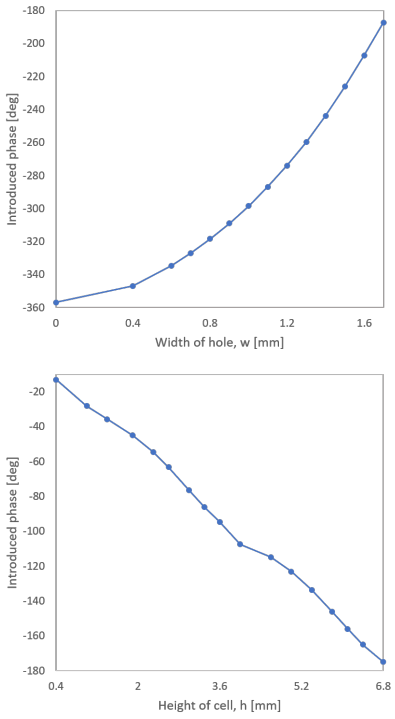

Fig. 14. Phase introduced by the cell versus width of the hole and height of the cell, respectively.

source, and the lens isn't infinite so doesn't account for edge effects. The simulations used the Frequency Solver Domain and two waveguide ports, one 10 mm away from the top and the other 10 mm from the bottom of the cell. The incidence angle was set to zero, and the perforation width of the the type 1 cell was changed with a parameter sweep of w from 0 to 1.7 mm, and the height of the type 2 cell was changed with a parameter sweep of h, from 0.4 to 14.1 mm, with a step size of 0.1 mm. The reason for the 0.8 mm difference between the cell length p and the hole length w is due to the nozzle diameter of 0.4 mm of the 3D printer. The value of the unwrapped phase of the resulting S_{21} parameter was obtained for each value of w and h and also for a cell of 14.2 mm height but completely made of vacuum, so the phase introduced by the unit cell was determined by $\phi_{cell} - \phi_{vacuum}$. The cells were picked so as to obtain a stepsize of around $10°$, resulting in 31 different cells in the $[-360°, 0]$ range. If close values of w or h had a close phase output the one which maximized the $|S_{21}|$ parameter was picked.

V. Full Wave Simulations of the Transmit-Array

In order to simulate the TA in full wave the models of the TA lens was designed by first assigning a phase shift to each cell, as explained in Section IV, second by assigning a phase shift for each point of the lens and finally generating the lens using a Visual Basic for Applications (VBA) macro for CST-MWS. Two different TA lenses were constructed, one for a spherical wave incidence, shown in Fig. 15, the other for a Gaussian beam incidence, shown in Fig. 16, to compare the performance of the two antennas.

The dimensions used for the design of the lens were the same for both lenses as in [2], that is, 195×145 mm.

The focal distance used to design both lenses was of $F = 110$ mm but instead of this being the distance from the source to the base of the lens, it is the distance to the middle of the lens thickness and thus the distance to the base is 102.9 mm. This was done because the main lobe at the central position was not symmetric as was expected, so a few adjustments in the lens position were experimented with to resolve this problem. This might have been due to the lens being quite thicker than what is usually used. Additionally, the TA lens is inverted (the base is facing away from the feed) also due to better results obtained from simulations.

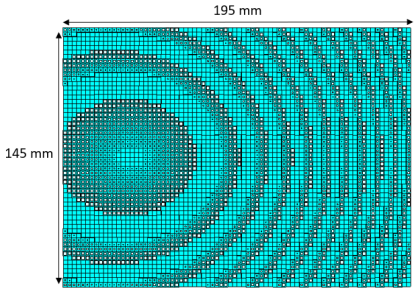

Fig. 15. Front view of the spherical wave TA lens model.

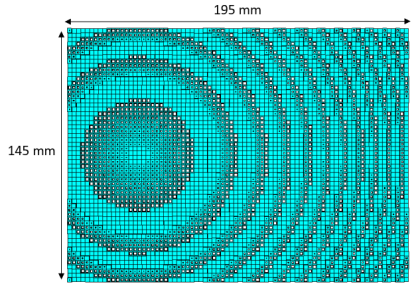

Fig. 16. Front view of the Gaussian beam TA lens model.

A. Spherical wave transmitarray

This TA is designed for a spherical wave feed and thus only the horn is used as the feed. The model is shown in Fig. 17, the distance from the horn to the base of the lens is 102.9 mm, as explained above.

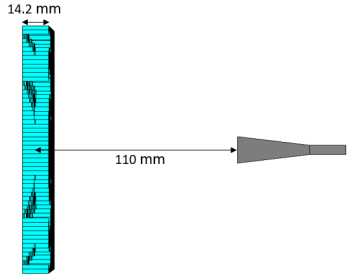

Fig. 17. Side view of the simulation model of the spherical wave TA

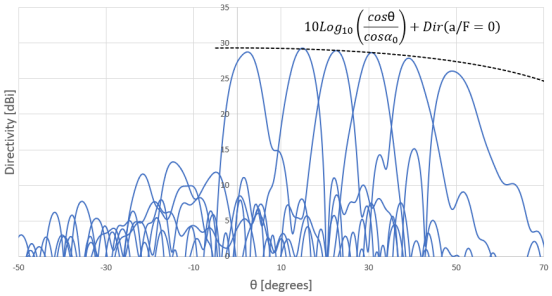

Fig. 18. Simulated farfield directivity radiation pattern for the spherical wave feed offset in the interval $a/F \in [-0.27, 0.55]$ with 0.09 step size. The dashed black curve represents the maximum normalized directivity as function of θ considering $\phi_{nl} = 0$.

Fig. 18 shows the directivity radiation pattern for the spherical wave TA. The dashed black curve represents the maximum normalized gain if nonlinear phase error was zero. The effect of beam aberrations in the positive feed displacements (tilt angles below 30 degrees) is not as obvious as in the results of the PO simulations shown in Fig. 3, as there doesn't seem to be any directivity decay, although some positions, in the whole interval, show high SLL on the main beam.

There is a lot of high side-lobe radiation being transmitted between -30 and 0 degrees, which will be addressed further.

B. Gaussian beam transmit-array

The model of the TA lens and the feed of the Gaussian lens and the horn were placed as shown in Fig. 19 to run a full-wave simulation in CST-MWS. The mouth of the horn is at a distance of 80 mm of the base of the Gaussian lens and at a distance of 110 mm of the center of the TA lens. As explained above, the focal distance of 110 mm is to the center of the lens, so the horn is 102.9 mm away from the TA lens instead of 110 mm and the lens is inverted.

Fig. 20 shows the simulated directivity radiation pattern. This TA produces a well defined main lobes and low SLL for feed offset different than zero. There is a lot of high sidelobe

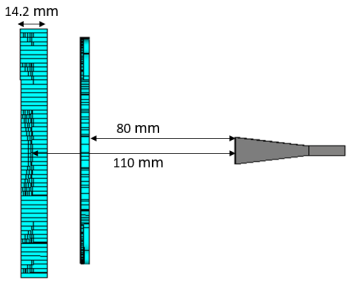

Fig. 19. Side view of the simulation model of the Gaussian beam TA

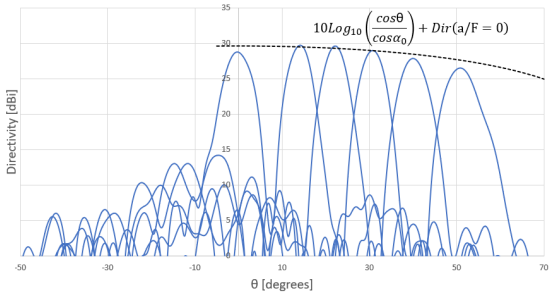

Fig. 20. Simulated farfield directivity radiation pattern for the Gaussian beam feed offset in the interval $a/F \in [-0.27, 0.55]$ with 0.09 step size. The dashed black curve represents the maximum normalized directivity as function of θ considering $\phi_{nl} = 0$.

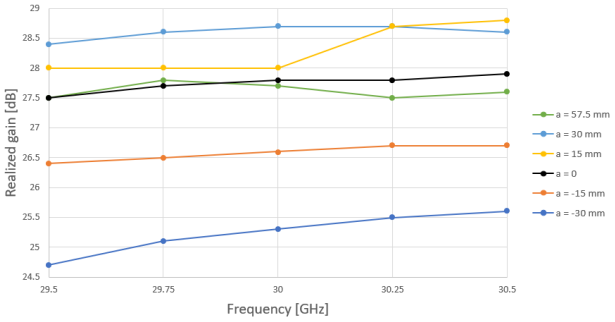

Fig. 21. Frequency responses of the main beam realized gain for different feed offsets.

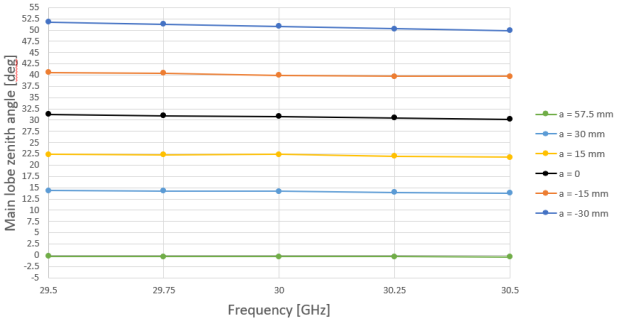

Fig. 22. Frequency response of the main beam tilt for different feed offsets.

radiation being transmitted in the $-30°$ and $0°$ zone, which is partly due to the large thickness of the TA lens.

The simulations above were also used to obtain the radiation

pattern for frequencies 1 GHz around the central frequency 30 GHz, in steps of 0.25 GHz. The gain against frequency responses for different feed offsets a is represented in Fig. 21 and the main lobe zenith angle versus the frequency in Fig. 22. Both frequency responses are fairly constant, with a difference lower than $|1|$ dB from the central position's gain and a difference lower than $|1.5|$ degrees from the central position's angle.

VI. Transmit-array measurement results

The prototype of the TA lens was fabricated using the same method described previously. Using the 3D Computer-aided design (CAD) models used in the simulations in Section V the TA lens prototype was 3D printed in PLA, with the dimensions, 195 mm $\times$ 145 mm and maximum and minimum thickness of 14.2 mm and 0.4 mm respectively. It was possible to obtain perforations from 0.1 to 0.7 mm although some imperfections might be present in the prototype as the nozzle used only permitted a precision of 0.4 mm and the extruded material did not always set evenly.

The 3D printed TA was mounted onto the support structure and the farfield radiation pattern was measured for the two horn polarizations, E and H fields. Fig. 23 shows the feed prototype in the anechoic chamber and Fig. 24 shows the simulated and measured H-plane farfield realized gain radiation pattern of the feed for 30 GHz and feed displacements from -30 mm to 57.5 mm. The feed displacement was achieved by sliding the TA lens along the support structure.

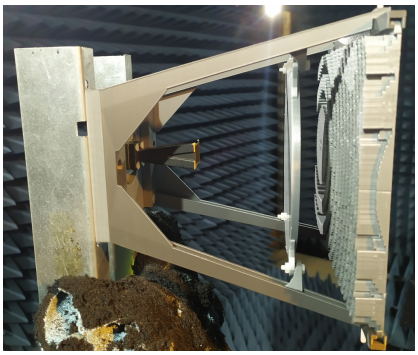

Fig. 23. TA prototype mounted in the anechoic chamber.

Comparing the simulated and measured results of the radiation pattern in Fig. 24 it can be seen that the TA behaves as expected. There are small changes encountered in the measured results. There is a slight difference in the tilt however it is consistent for all the positions so it is most likely due to a misalignment in the prototype model. Some aberrations can be seen but not very high. The gain is also lower but that is to be expected due to inaccuracies in the manufacturing and assembling of the prototype and unaccounted losses in the simulations.

The simulations show a scan loss of 3.5 dB for 29.5 GHz and 3.3 dB for 30 GHz. The measurements show a worse scan loss of 4.5 dB for 29.5 GHz and 3.8 dB for 30 GHz. The

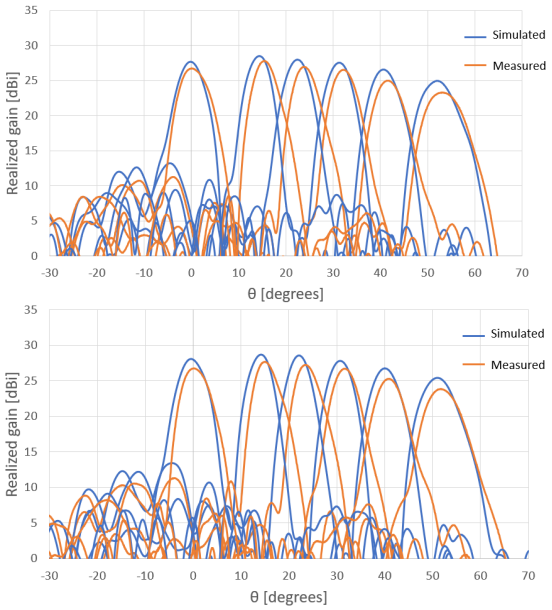

Fig. 24. Simulated and measured farfield realized gain of the TA at 29.5 and 30 GHz, respectively.

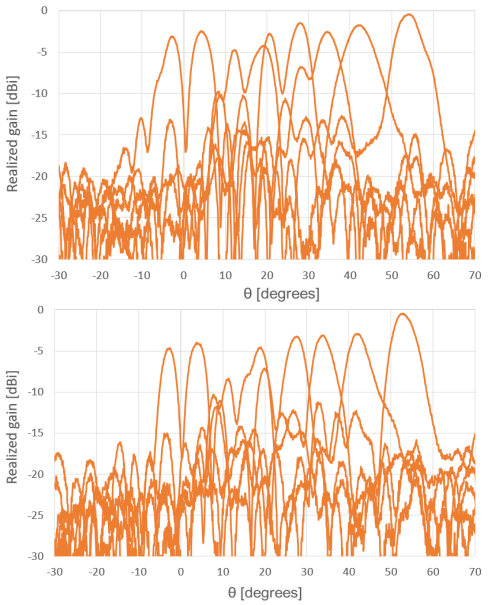

Fig. 25. Measured cross component farfield realized gain of the TA at 29.5 and 30 GHz, respectively.

maximum values of the measured cross component, shown in Fig. 25, are at least 20 dB inferior to the co component.

VII. Conclusion

The objective of this thesis was the design and fabrication of a TA antenna working at the satellite uplink [29.5-30.0] GHz and capable of being 3D printed and provide beam steering up to 50 degrees. Its particularity was the use of a Gaussian beam as the source and formulation of the phase compensation for the design of the main lens, with the objective of eliminating

or greatly reducing beam aberrations and SLL resulting from beam steering, compared to other solutions in the literature. The proposed solution was first analysed using a PO program and Mathematica and then designed, modeled and simulated using Mathematica and CST-MWS.

The chosen primary feed was obtained after designing and testing various lenses at different focal distances and dimensions such as to eliminate phase jumps and to obtain a thin lens and reduce beam deformity and reflections between this lens and the main one. The round lens has a radius of 67.5 mm and a minimum and maximum thickness of 0.3 mm and 4 mm respectively, and is at a focal distance of 80 mm from the horn antenna. It was possible to produce a Gaussian beam, the simulations of this feed show good agreement with the ideal Gaussian beam macro from CST-MWS, although the radiation pattern of this feed shows some distortion and a bump in the 0 degrees direction which lowers the directivity slightly. The prototype was fabricated in the IT facilities by 3D printing, as was the support structure for the two lenses, and the measurements showed good agreement with the simulations, for the [29.5-30.0] GHz band.

The TA lens was designed to compensate the phase of a Gaussian beam and have the fixed dimensions of 195 x 145 mm. It took several iterations to reach the final solution, experimenting with different cell dimensions, focal distances and lens positioning, as although the lens was designed for a focal distance F of 110 mm, it was positioned at a distance of 102.9 so the middle of the lens is at the 110 mm distance. The lens was also flipped. These adjustments were made because the radiation pattern showed an asymmetric main lobe in the central position, which was resolved. Some time was also dedicated to understanding the cause and attempting to eliminate the high radiation seen in the -20 to 0 degrees zone. It was concluded it was mostly due to the thickness of the lens, 14.2 mm at the thickest, as simulations with a higher permitivity and lower thickness greatly reduced this problem. In the end it was possible eliminate beam aberrations and lower SLL in the simulations in CST-MWS for a scanning range up to 51 degrees, although the scan loss was higher than seen in the literature. The prototype was also fabricated in the Instituto de Telecomunicacões (IT) facilities by 3D printing and its measurements showed some aberrations but much lower than seen in the literature and otherwise showed good agreement with the simulations.

The overall antenna dimensions, including the support structure, were 195 x 175.4 mm and a height of 178.6 mm. At 30 GHz the simulated antenna has a maximum gain of 28.7 dBi, scan loss of 3.3 dB, scanning range of 51.4 degrees and SLL below -20 dB for all simulated feed displacements. The measured antenna has a maximum gain of 27.7 dBi, scan loss of 3.8 dB, scanning range of 51.6 degrees and SLL below -19 dB measured feed displacements except for one, below -16 dB.

VIII. Future Work

It was proven that a Gaussian beam source TA reduces beam aberrations and SLL. This conclusion can be used as a starting point for a future work to improve scan loss, side lobe radiation in a non desired direction and overal antenna dimensions. The main lens is quite thick due to the material used, and the cells have a high transmission loss. Other types of unit cells can be used to reduce the lens thickness and thus improve transmission loss and reduce the high radiation seen in the -20 to 0 degrees zone, such cells made of material with a higher permitivity or layered unit cells made from a combination of dielectric material and printed patches as seen in [2] or others, although most likely this would make fabrication more complex.

Antenna height is also not optimal and could be reduced using a more compact feed capable of producing a Gaussian beam.

Acknowledgment

I would like to thank my thesis advisors Professor Carlos A. Fernandes, of Instituto Superior Técnico, and Professor Sérgio A. Matos, of Instituto Superior de Ciências do Trabalho e da Empresa, for giving me this opportunity and helping me throughout its execution, and Instituto de Telecomunicações Researcher João Felício and Laboratory Technician António Almeida for their help and prototype construction and measurements. I also would like to thank Instituto de Telecomunicacões, UIDB/50008/2020, and project ADAM3D: PTDC/EEITEL/30323/2017, for financing all the needed material used in this thesis, and for the usage of IT laboratories, software and hardware equipment.

References

[1] ITU, "Evolving satellite communications," *ITU News Magazine*, no. 2, p. 9, 2019. [Online]. Available: https://www.itu.int/en/myitu/Publications/2020/04/02/19/54/ITU-News-Magazine-No-2—2019

[2] E. B. Lima, S. A. Matos, J. R. Costa, C. A. Fernandes, and N. J. Fonseca, "Circular Polarization Wide-Angle Beam Steering at Ka-Band by In-Plane Translation of a Plate Lens Antenna," *IEEE Transactions on Antennas and Propagation*, 2015.

[3] C. A. C. Fernandes, "Kh3d near. users manual, version 0.2h," Insituto de Telecomunicações - IST, Tech. Rep., 2018.